energy&fuels

pubs.acs.org/EF

Article

Hydrodeoxygenation of Isoeugenol over Carbon-Supported Pt and Pt−Re Catalysts for Production of Renewable Jet Fuel

Mark E. Martínez-Klimov, Päivi Mäki-Arvela, Zuzana Vajglova, Moldir Alda-Onggar, Ilari Angervo, Narendra Kumar, Kari Eränen, Markus Peurla, Mehmet Harbi Calimli, Joseph Muller, Andrey Shchukarev, Irina L. Simakova, and Dmitry Yu. Murzin*

Cite This: *Energy Fuels* 2021, 35, 17755−17768

Read Online

ACCESS | Metrics & More | Article Recommendations

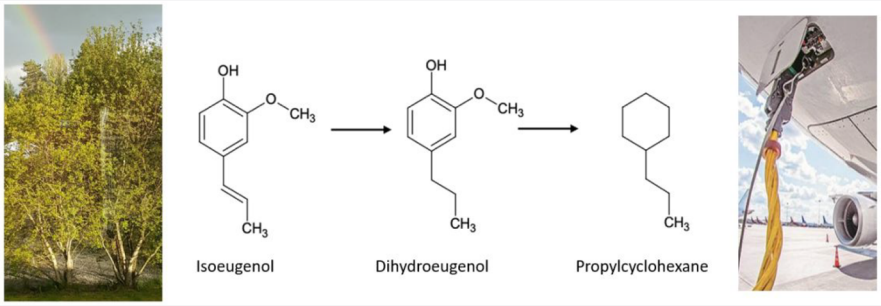

ABSTRACT: A series of monometallic platinum and bimetallic platinum−rhenium catalysts supported on mesoporous carbon Sibunit, which is a type of mesoporous, microcrystalline carbon, were investigated for hydrodeoxygenation (HDO) of isoeugenol (IE) at 200−300 °C and 30 bar of H_2, using dodecane as a solvent. Catalytic activity was tested in a batch reactor to screen the catalysts and, for comparison, also in the continuous mode. For batch experiments, complete conversion, and a high yield of the desired product, propylcyclohexane (PCH), were obtained for all bimetallic PtRe/Sibunit in 240 min, with the highest yield of PCH when Pt:Re ratio was 1:1 or 1:3. The results for Pt−Re (1:1) were reproducible, in terms of catalytic activity and reusability of catalysts, which showed no deactivation. Monometallic Pt catalysts displayed low activity. Continuous experiments were performed with PtRe(1:1)/Sibunit at 30 bar H_2, 0.5 mL/min of the liquid flow, and temperatures between 75 °C and 200 °C. The distribution of products showed deoxygenation at higher temperatures, while at lower temperatures, mainly oxygenated products were formed. XPS results confirmed the presence of ReOx species, where an increase in the platinum loading resulted in a decrease in the fraction of ReOx species and subsequently lower PCH yield.

INTRODUCTION

Fossil-derived fuels still provide most of the energy used worldwide, with its consumption still increasing yearly.[1] This constant increase of greenhouse gases emissions, depletion of nonrenewable resources, and alternative-fuel regulations have promoted the development of new technologies and processes to solve these challenges.[2]

While the use of electric and hybrid vehicles has increased considerably in recent years, these technologies are not appropriate for their use on commercial airplanes, mainly because of insufficient electrical storage as well as the weight of batteries and electric propulsion systems.[3] Therefore, biomass, being a renewable and sustainable feedstock alternative to such fossil feedstock as crude oil, has attracted much attention as a source for production of fuels and chemicals.[4]

One of the main conversion processes to obtain bio-oil is the pyrolysis of lignocellulosic biomass. The obtained bio-oil is rich in oxygenated compounds, making it unsuitable as a fuel, because of, for example, high viscosity, a low heating value, high acidity, and chemical instability.[5] Bio-oil requires additional steps to be able to obtain biofuels[6] that could substitute or supplement those currently in use.[7] One of the main routes for upgrading biomass-derived oil into liquid fuels is through hydrodeoxygenation (HDO).[8] In HDO, oxygen is removed from organic molecules as water, CO_2, or CO, in the presence of a catalyst and hydrogen.

Bifunctional catalysts with two types of active sites are required for HDO: one site to activate hydrogen (metal), and another one to activate oxygen (oxophilic metal or acid

Received: August 3, 2021
Revised: September 20, 2021
Published: October 18, 2021

https://doi.org/10.1021/acs.energyfuels.1c02656
Energy Fuels 2021, 35, 17755−17768

support). Hydrogenation, dehydrogenation, hydrocracking, and decarbonylation occur on metal sites, while dehydration, isomerization, and hydrogenolysis occur on the acid sites.[9] Monometallic catalysts deposited on oxide supports and carbon have been extensively studied for the HDO of various model compounds.[10] The most common catalysts are noble[11] (such as Pt, Rh, Pd), or transition metals[12] (such as Ni, Co, Mo) supported on zeolites,[13] or oxides (e.g., Al_2O_3[14] and SiO_2[15]). Bimetallic catalysts mainly studied for HDO include Mo in combination with Ni and Co,[16] which have been traditionally used for HDO processes in petroleum refining. Bimetallic catalysts containing noble metals and rhenium (RuRe/C,[17] IrRe/SiO_2,[18,19] RePd/CeO_2,[20] IrRe/Al_2O_3[14]) have shown that the presence ReOx resulted in activity elevation. While Re has been mainly studied in the context of catalytic reforming and aqueous phase reforming, the interest in rhenium has expanded to other reactions, where the oxophilic nature of the metal could improve catalytic activity.

Studies have found that oxides of Mg, Mo, W, and Fe can enhance HDO by improving the reducibility of Pt species through an electron transfer.[21] DFT calculations have also proved a synergistic effect between Pt and MOx species in adsorbing/activating C−O bonds, making metal−metal oxide catalysts interesting and promising for HDO.[22]

The use of new supports such as nanotubes,[23] ordered-mesoporous silica,[24,25] and different types of carbon,[26] has attracted the attention of researchers, because of their properties, such as high surface area, porosity, acidity, or basicity, etc. Among such supports, Sibunit, which is a type of mesoporous, microcrystalline carbon, is considered as an attractive material, because of its high mechanical strength,[27] reasonably large surface area, high purity, and chemical stability,[28] combining the properties of graphite and activated carbon. Additional benefits of Sibunit-based catalysts are that they can be produced in large scale and in different shapes, such as whole and hollow cylinders, rings, etc., allowing for a wide range of applications.[29] This material is synthesized via the deposition of pyrolytic carbon from C_1−C_3 hydrocarbons on granulated carbon black, followed by condensation and steam activation.[30] Temperature-programmed desorption (TPD) studies of Sibunit have reported that CO and CO_2 evolutions resemble those for other various carbonaceous materials, with a high amount of carboxylic groups on the surface.[31]

Currently, most HDO is performed on a laboratory scale, using three-phase systems (gas−liquid−solid) in batch reactors. While this approach gives information regarding kinetics, industrial interest focuses on continuous flow processes, which allow for scalability, higher and constant throughput, and improved automation.[32]

Studies on HDO in continuous reactors have mostly centered on guaiacol;[19,33,34] however, isoeugenol has not been studied previously in this type of systems. Isoeugenol is a model compound of interest, as its structure is representative of the three phenylpropane units that constitute lignin.[35] Its molecular structure also contains the main oxygenated groups, more specifically, the hydroxyl, methoxy, and allyl groups found in the compounds of lignin-derived bio-oil.

Research focused on the HDO of isoeugenol using bimetallic catalysts—in particular, bimetallic Pt−Re—in both batch and continuous reactors has been scare. Our previous research on isoeugenol HDO was focused on Ir, Pt, and Re catalysts supported on alumina, highlighting the importance of an oxophilic metal for the reaction.[13] Another investigation of Ir and Ni catalysts supported on ZrO_2 resulted in the formation of large amounts of gas-phase products, therefore giving a low mass balance closure in the liquid phase.[36]

The purpose of this work was to study HDO of isoeugenol using monometallic Pt and bimetallic Pt−Re supported on carbon as catalysts in a batch reactor. Furthermore, HDO of isoeugenol was investigated for the first time in a continuous reactor.

EXPERIMENTAL SECTION

Chemicals. The following chemicals were acquired commercially: isoeugenol (98%, mixture of *cis* and *trans*, Aldrich), dihydroeugenol (≥99, Sigma−Aldrich), *n*-dodecane (≥99%, Acros Organics), benzene (≥99%, Sigma−Aldrich), propylcyclohexane (99%, Aldrich) cyclohexane (99.9%, Alfa Aesar), hexane (>97%, Sigma−Aldrich), tetraammineplatinum(II) nitrate (≥50.0% Pt basis, Aldrich). H_2PtCl_6 (Kraszvetmet, Krasnoyarsk, Russia) and $HReO_4$ (20 wt %, Reachim, Russia).

The following gases were used: hydrogen (AGA, 99.999%), argon (AGA, 99.999%), and helium (AGA, 99.996%).

Preparation of Catalysts. The following catalysts were acquired from Degussa: F106XKYF and F1525XKT. The notation given to these catalysts was Pt/C1 and Pt/C2, respectively, both containing up to 5 wt % Pt on activated carbon.

Activated carbon Norit was supplied by NORIT (NORIT R 3 EXTRA activated carbon) and Sibunit was supplied by the Boreskov Institute of Catalysis, Siberian Branch of the Russian Academy of Sciences.

Monometallic Pt catalysts, Pt/Norit, and Pt/Sibunit were synthesized by the incipient wetness impregnation of tetraammineplatinum(II) nitrate (≥50.0% Pt basis, Aldrich) on Norit or Sibunit, the catalysts were denoted as Pt/Norit and Pt/Sibunit, respectively.

Bimetallic Pt−Re catalysts (PRC series; PRC11, PRC31, and PRC13) were synthesized by impregnation. Sibunit (<63 μm) was impregnated with an aqueous solution of a mixture of the metal precursors H_2PtCl_6 (OAO Aurat, Russia) and $HReO_4$ (20 wt %, Reachim, Russia). Three bimetallic catalysts with different metal ratios were prepared: 1:1 with the nominal metal loading of each metal of 4 wt %, 1:3 with the nominal metal loading of 2 wt % for Pt and 6 wt % for Re, and 3:1 with the nominal metal loading of 6 wt % for Pt and 2 wt % for Re. The catalysts were named PRC11, PRC13, and PRC31, respectively.

Granulated PRC11 catalyst used for the continuous reactor experiments was prepared by the same method as described above, only using larger particles of Sibunit (1 mm).

After impregnation, the catalysts were calcined at 110 °C overnight, reduced in a hydrogen flow with a temperature ramp of 2 K/min until 330 °C, and kept at the final temperature for ca. 6 h.

The catalysts used in the batch reactor were reduced ex situ under hydrogen flow (40 mL/min) at 350 °C for 3 h (10 °C/min) prior to experiments. After reduction, the catalyst was flushed with argon and the solvent was added to avoid reoxidation of the catalyst. The catalyst used in the continuous reactor was reduced in situ under the same conditions as with the catalysts used in the batch reactor.

A summary of the catalysts used in the current work is presented in Table 1.

Reactor Setup and Analysis. HDO of isoeugenol was performed as a model reaction to determine the activity of Pt and Pt−Re catalysts supported on carbon. The reactions were performed in a 300 mL stainless steel batch reactor (PARR Instruments) equipped with a mechanical stirrer. The samples were taken at regular time intervals. The stirring speed was set to 900 rpm to avoid external mass-transfer limitations. The size of the catalyst particles was <63 μm, to ensure the absence of internal mass-transfer limitations. For HDO of isoeugenol, 0.05 g of the catalyst, 0.1 g of the reactant, and 50 mL of dodecane were used. The liquid samples were analyzed by gas

https://doi.org/10.1021/acs.energyfuels.1c02656
Energy Fuels 2021, 35, 17755−17768

Table 1. Summary of Catalysts Used for HDO of Isoeugenol

	Catalyst			
denomination	metal	loading (wt %)	support	type
Pt/C1	platinum	5	activated carbon	commercial (Degussa)
Pt/C2	platinum	5	activated carbon	commercial (Degussa)
Pt/Norit	platinum	2	activated carbon	self-synthesized
Pt/Sibunit	platinum	4	mesoporous carbon	self-synthesized
PRC11	platinum, rhenium	4 and 4	mesoporous carbon	self-synthesized
PRC31	platinum, rhenium	6 and 2	mesoporous carbon	self-synthesized
PRC13	platinum, rhenium	2 and 6	mesoporous carbon	self-synthesized
PRC11 granulated	platinum, rhenium	4 and 4	mesoporous carbon	self-synthesized

chromatography (GC) and gas chromatography/mass spectroscopy (GC/MS). In GC analysis, a DB-1 capillary column (Agilent, Model 122-103e) of 30 m length, 250 μm internal diameter and 0.5 μm film thickness was utilized. Helium was applied as a carrier gas with the flow rate of 1.7 mL/min. The temperature program for GC analysis was as follows: 60 °C (5 min), 3 °C/min to 135 °C, and 15 °C/min to 300 °C. GC-MS analysis was performed over the same column and using the same temperature program as used in GC.

Continuous experiments were performed in a laboratory-scale fixed-bed reactor with the following dimensions: 12 cm length, 1.2 mm inner diameter, 70-mm catalyst zone, 3-mm thermocouple pocket. The reactor was loaded with 0.3 g of the catalyst mixed with 15 g of fine granular quartz (200−800 μm) to have a uniform distribution of the catalyst throughout the catalytic bed; the remaining space was filled with quartz. The reaction mixture was fed downflow via a high-performance liquid chromatography (HPLC) pump (Knauer Smartline). The reaction conditions were as follows: 30 bar H_2, gas flow rate of 0.5 mL/min, liquid flow rate of 0.5 mL/min, temperatures between 75 and 200 °C. The catalyst was reduced in situ at 350 °C for 3 h (temperature ramp = 10 °C/min) under a hydrogen flow rate of 40 mL/min at atmospheric pressure. The liquid samples taken periodically during 4 h were analyzed using the same procedure as that used with the batch reactor.

Catalyst Characterization. Textural properties of the catalysts were determined using nitrogen physisorption (Micrometrics, Model 3Flex-3500). The Dubinin−Radushkevich method was used to determine the specific surface area while the pore size distributions were obtained with the Barrett−Joyner−Halenda (BJH) approach, using desorption data and density functional theory (DFT) method. Prior to the measurements the catalysts were outgassed ex-situ under vacuum and 180 °C for 20−24 h in a Micromeritics VacPrep 061 Sample Degas System. Thereafter, they were degassed in situ for 4 h at 180 °C.

Surface acidity was determined in accordance with the studies found in the literature focusing on carbon-supported catalysts.[37−41] It was determined by measuring the pH of a slurry consisting of 50 mg of the catalyst and 50 mL of distilled water under agitation with a magnetic stirrer. The pH of the slurry was determined using a Mettler Toledo pH electrode.[42]

X-ray diffraction (XRD) reflexes of catalysts were recorded with an X-ray diffractometer (Model D8, Bruker, Germany) using Cu K radiation and a LynxEye detector by scanning with a step of 0.05° and an accumulation time of 3 s at each point with a slit width of 0.26° or accumulation time of 1 s at each point with a slit width of 0.52°.

Scanning electron microscopy (SEM) was utilized to obtain information on the morphology of supports and catalysts. A Zeiss Leo Gemini 1530 microscope, combined with secondary electron and backscattered electron detectors, was applied. An acceleration voltage of 15 kV was used for the X-ray analyzer.

Transmission electron microscopy (TEM) was utilized to determine the metal particle size and study the morphology and porosity. The equipment used for analysis was a Model JEM-1400Plus system (JEOL, Japan) with a maximal acceleration voltage of 120 kV. The interpretation of TEM images and determination of particle sizes of the fresh and spent catalysts were done using the ImageJ program.

Prior to the TEM analysis, the samples were ground and suspended in ethanol. A drop of suspension was mounted on a copper grid coated with a carbon film and the solvent evaporated. The particle size distribution of metal particles was determined by measuring the diameter (d) of more than 300 particles visible in TEM micrographs.

Temperature-programmed reduction with H_2 (TPR) was performed in an AutoChem 2910 instrument. An amount of 0.1 g of catalyst was dried at 120 °C for 1 h, followed by reduction with 5 vol % hydrogen in argon, using the following temperature program: 25−700 °C at 10 °C/min. A thermal conductivity (TC) detector was used, and the cooling system, containing liquid nitrogen and a 2-propanol mixture, was applied to dry the gas-phase samples before entering the TC detector.

X-ray photoelectron spectroscopy (XPS) measurements were performed ex situ with an Axis Ultra DLD electron spectrometer manufactured by KRATOS Analytical, Ltd., using monochromated Al Kα excitation source.

Table 2. Textural Properties, Metal Particle Sizes, and pH of Slurries of Catalysts and Supports

	Textural Characteristics						
				D_P (nm)			
catalyst	SSA[a] (m^2/g)	V_Σ (cm^3/g)	V_{MP} (cm^3/g)	BJH	DFT	metal particle size (nm)	pH of slurry
Norit	1247	0.58	0.51	4	0.6−0.7	−	7.5
Sibunit	330	0.52	0.09	4	0.9, >3.5	−	6.5
Pt/C1	450	0.29	0.17	4	0.6−0.7	3.1	5.7
Pt/C2	421	0.28	0.16	4	0.6−0.7	2.9	4.9
Pt/Norit	857	0.39	0.31	4	0.6−0.7	4.2	7.1
Pt/Sibunit	283	0.35	0.08	4	0.9, >3.5	3.5	6.6
PRC11	268	0.31	0.07	4	0.9, >3.5	1.3	6.0
PRC11 (used)	222	0.23	0.04	4	0.9, >3.5	1.5	−
PRC31	277	0.34	0.08	4	0.9, >3.5	1.2	6.1
PRC13	275	0.32	0.08	4	0.9, >3.5	1.3	6.0
PRC11 granulated	234	0.32	0.07	4	0.9, >3.5	1.4	6.0
PRC11 granulated (used)	176	0.25	0.05	4	0.9, >3.5	1.7	−

[a]Specific surface area.

https://doi.org/10.1021/acs.energyfuels.1c02656
Energy Fuels 2021, 35, 17755−17768

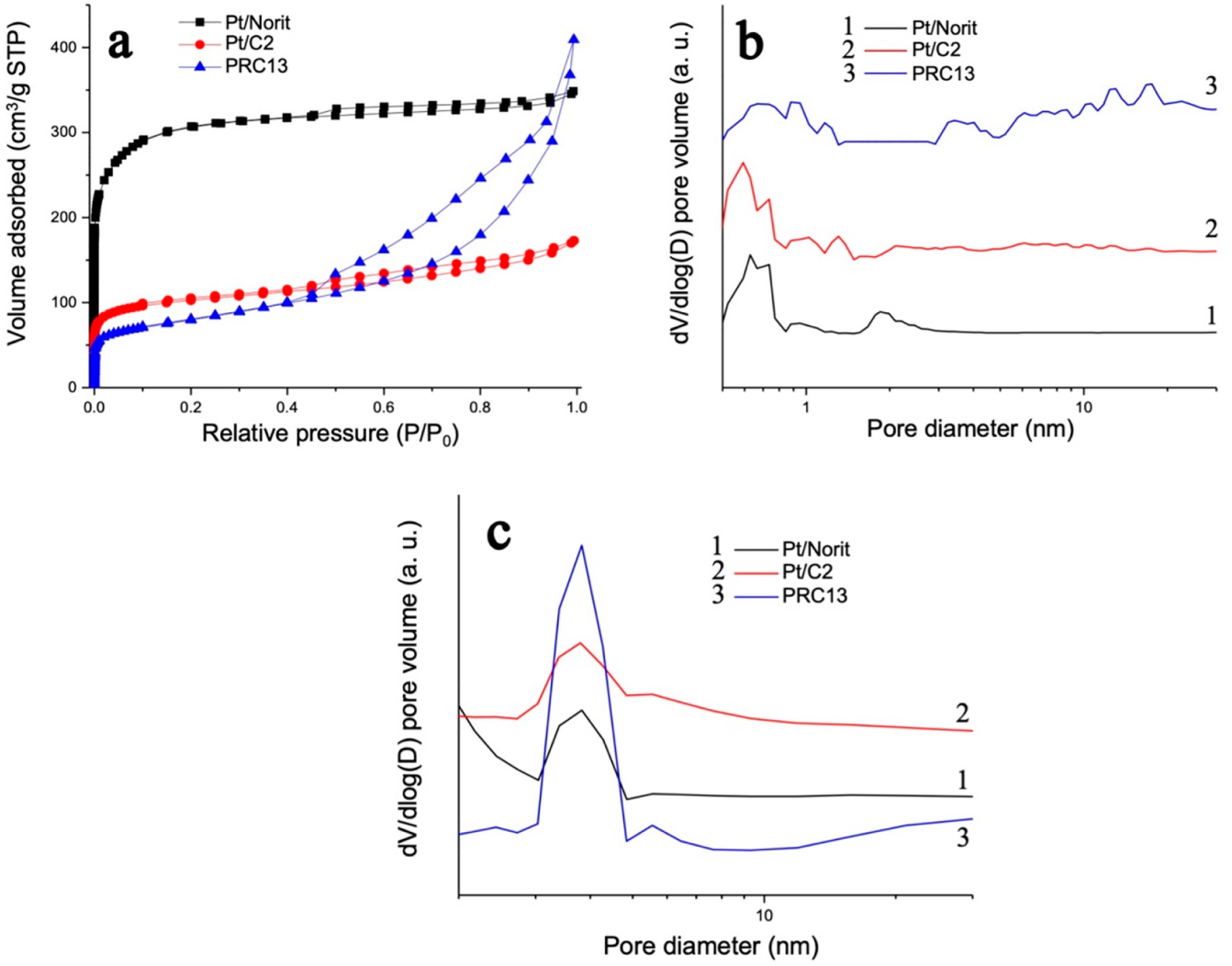

Figure 1. (a) Adsorption−desorption isotherm, (b) DFT pore size distribution, and (c) BJH pore size distribution of Pt/Norit, Pt/C2, and PRC13 catalysts.

RESULTS AND DISCUSSION

Catalyst Characterization. A summary of the textural properties, metal particle sizes, and pH of the catalysts and supports slurries is presented in Table 2. Results will be discussed in the following sections.

Nitrogen physisorption results (Table 2) show that deposition of Pt resulted in a slight decrease of the textural properties for all catalysts, which can be explained by blocking of the pores by the metal. The highest specific surface area (SSA), total pore volume (V_{Σ}) and the micropore volume (V_{MP}) were recorded for C_{NORIT} and the corresponding catalyst Pt/Norit. On the other hand, the catalysts supported on mesoporous Sibunit (Pt/Sibunit and PRC series) showed lower SSA, V_{Σ}, and V_{MP}.[43] The addition of Re had a very low effect on the textural properties of PRC catalysts. Commercial catalysts Pt/C1 and Pt/C2 showed properties similar to those of Norit, all being supported on activated carbon.

Catalysts supported on Sibunit had much lower V_{MP} values (<1 cm^3/g), when compared to catalysts supported on activated carbon (>0.15 cm^3/g), and the adsorption isotherms and the pore size distribution indicated its mesoporous characteristics.

Three different types of catalysts are compared in Figure 1, including adsorption−desorption isotherms (Figure 1a) and the pore size distributions obtained by DFT (Figure 1b) and BJH (Figure 1c).

Catalysts supported on activated carbon showed the isotherm of type I and hysteresis type H4, indicating the presence of micropores characteristic activated carbons, according to the IUPAC classification.[44]

On the other hand, all catalysts supported on Sibunit showed a combination of isotherm types I and IV, indicating the presence of both micropores and mesopores, and H3 hysteresis. Pore size distribution obtained by DFT (Figure 1b) exhibited a main pore contribution between 0.6 and 0.7 nm for catalysts supported on Norit and both Pt/C1 and Pt/C2. Pore size distribution obtained by BJH (Figure 1c) exhibits a narrow main pore contribution for all samples at ca. 4 nm.

For PRC catalysts, the main peak present in the microporous range was between 0.9 nm and 1.1 nm; however, more porosity was present at >3.5 nm, indicating mesoporosity.[27]

The spent PRC11 catalysts used in batch and continuous reactors were characterized by nitrogen physisorption. The results (Table 2, Figure 2) show that surface area decreased after the reaction for both cases. This could be due to

https://doi.org/10.1021/acs.energyfuels.1c02656
Energy Fuels 2021, 35, 17755−17768

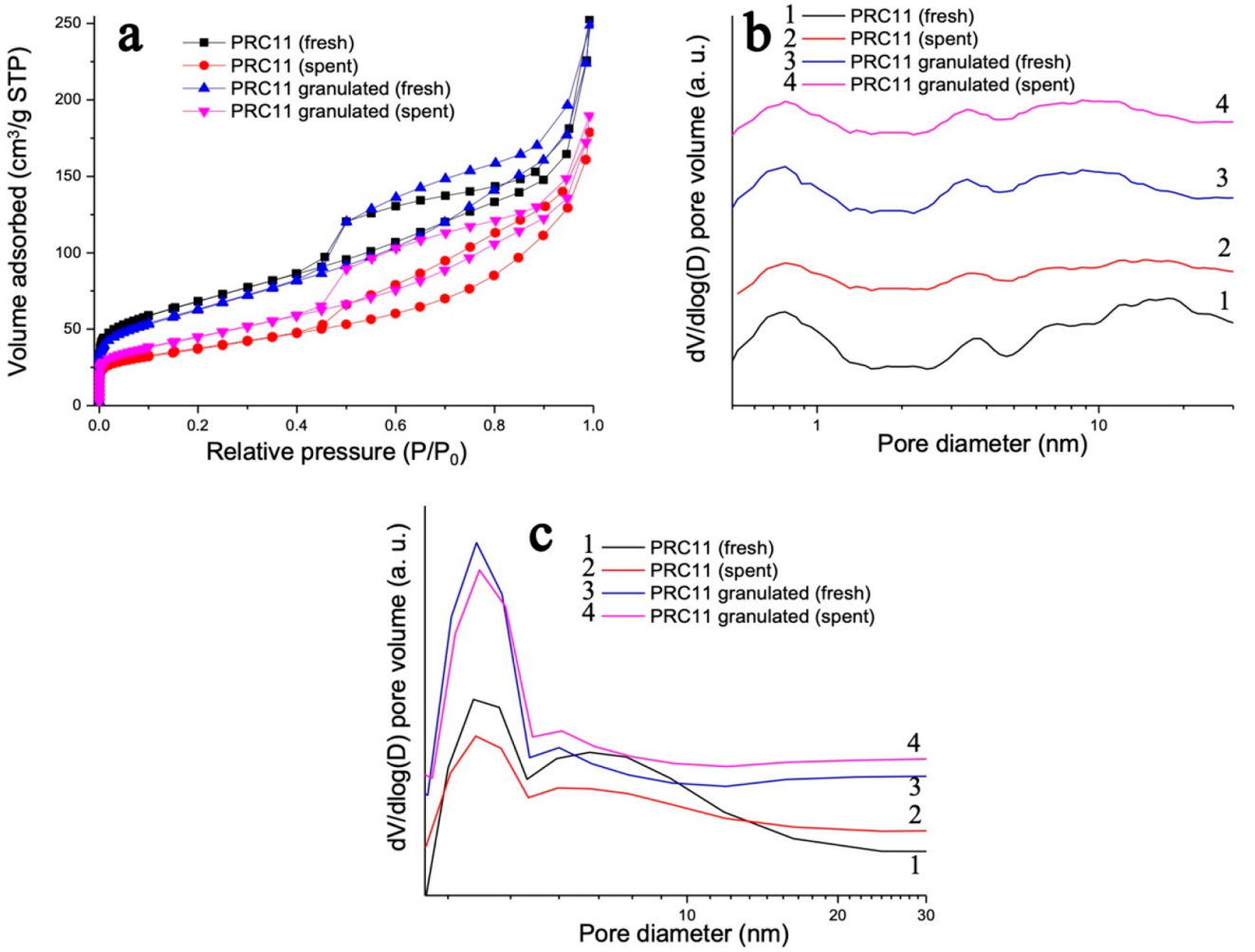

Figure 2. (a) Nitrogen adsorption−desorption isotherms, (b) DFT pore size distribution, and (c) BJH pore size distributions for the fresh, spent, and granulated PRC11.

formation of carbonaceous species that remained on the surface of the catalysts. Pore size distribution (Figures 2b and 2c) showed no changes in pore diameter, indicating low mechanical degradation.

The relative acidity of different catalysts shown in Table 2 indicates that both commercial catalysts exhibited high acidity when compared to the rest, with Pt/C2 being the most acidic catalyst of all (pH 4.9). The pH of the slurry was also measured for the pure supports Norit and Sibunit, where Sibunit displayed the lower pH value (pH 6.5). A slight decrease in pH was observed after deposition of Pt. All bimetallic PRC catalysts showed very similar pH values (pH ∼6), indicating that the addition of Re did not affect acidity considerably.

Pt peaks at ∼39.5°, 46°, 67°, and 81° (Figure 3) are attributed to the (111), (200), (220), and (311) reflections.[45] The presence of these peaks can be attributed to larger metal particles not considered or observed in TEM. Peaks at 26° and 42° belong to the carbon support, indicating presence of the microcrystalline structures.[46,47] The lack of peaks belonging to Re could be caused by high dispersion of Re particles or an overlap with carbon reflections.[48]

The lack of Pt peaks in PRC11 shows that the addition of Re improved Pt dispersion. As Figure 3 shows, the best Pt−Re ratio is 1:1, since Pt peaks are present for both PRC13 and PRC31.

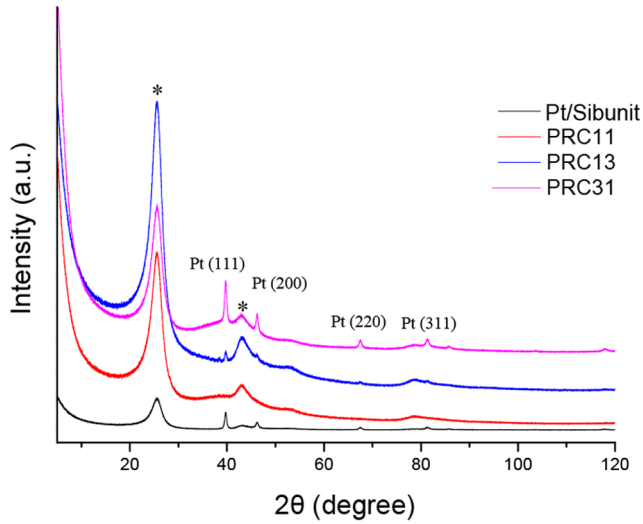

Figure 3. XRD diffractogram comparison of monometallic Pt/Sibunit and bimetallic PRC catalysts. Asterisk symbol (*) denotes signals for the Sibunit support.

https://doi.org/10.1021/acs.energyfuels.1c02656
Energy Fuels 2021, 35, 17755−17768

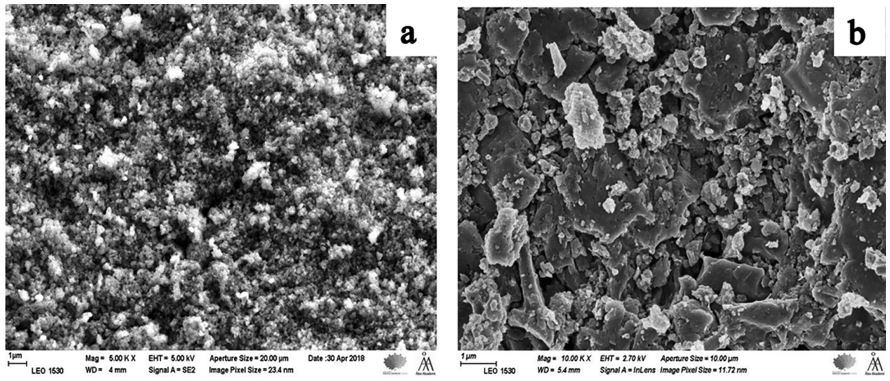

Figure 4. SEM micrographs of (a) Sibunit and (b) Norit.

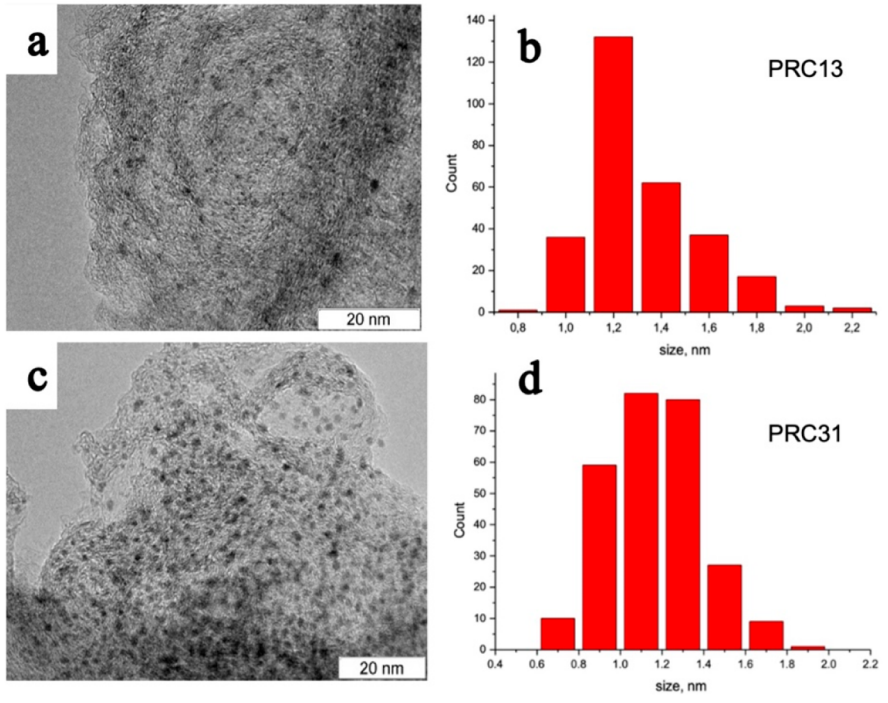

Figure 5. TEM micrographs and the metal particle size distribution of (a, b) PRC13 and (c, d) PRC31.

SEM analysis allows one to observe the morphological differences between Sibunit and Norit (Figure 4). It is possible to see that the structure of Sibunit consists of more-uniform granules (0.3−0.5 μm), while Norit is composed of more-heterogeneous and varied particles with sizes exceeding 0.5 μm.

TEM images of the reduced catalysts allow one to determine the metal particle size and the morphology of the catalysts with the results given in Table 2.

As can be seen from this table, all catalysts exhibited the metal particle sizes of <5 nm. The smallest metal particles and the highest metal dispersion were found in the PRC series (<1.4 nm), despite higher total metal loadings. In addition, PRC series showed a smaller metal particle size than monometallic Pt/Sibunit, indicating that the addition of Re helped to stabilize the metal particles on the surface of the support.[49]

Commercial catalysts presented similar particle sizes, ∼3 nm in size, while synthesized monometallic catalysts, Pt/Norit, and Pt/Sibunit exhibited the largest metal particle sizes.

For bimetallic PRC series, it was not possible to differentiate between Pt and Re nanoparticles; therefore, the combined metal particle size distributions and TEM micrographs for two PRC catalysts are presented in Figure 5.

A comparison of the TEM images (Figure 6) between the fresh and the spent PRC11 catalysts shows almost no changes in the particle sizes after the reaction, indicating good stability of metal particles.

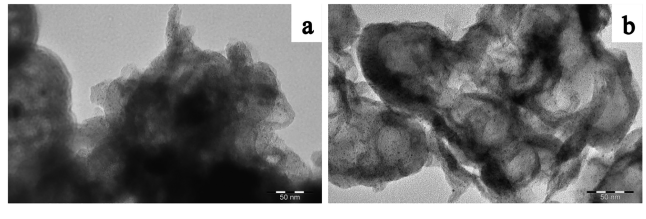

Figure 6. TEM micrographs of (a) fresh PRC11 and (b) spent PRC11.

https://doi.org/10.1021/acs.energyfuels.1c02656
Energy Fuels 2021, 35, 17755−17768

Reduction profiles for the PRC series of catalysts (Figure 7, Table 3) display two main peaks, namely, the first one at low temperatures (85−150 °C) and the second at higher temperatures (440−550 °C).

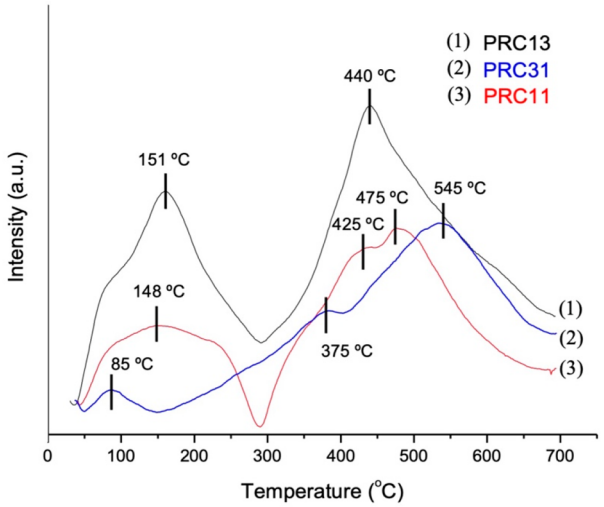

Figure 7. TPR profiles of bimetallic PRC11, PRC13, and PRC31 catalysts.

Table 3. Results from Hydrogen TPR

catalyst	$T_{max}1$ (°C)	$T_{max}2$ (°C)	total area (a.u.)
PRC11	148	475	96.6
PRC31	85	545	94.7
PRC13	151	440	165.6

Reduction peaks of monometallic platinum supported on carbon have been reported in the range of 150−300 °C,[50] whereas, for Re reduction, temperatures are higher, between 250 °C and 450 °C.[51] The peaks observed at 85−150 °C correspond to complete reduction of Pt, while those at 375 °C for PRC31 and at 425 °C for PRC11 are consistent with the results reported for the reduction of Re species supported on carbon.[51] However, broad peaks at higher temperatures (500−800 °C) attributed to methane formation, coming from the reaction of the carbon support with hydrogen, overlap with those of Re, making analysis challenging.

Shifts in the reduction temperatures have also been reported due to formation of Pt−Re alloy.[39−42] Migration of ReOx species toward reduced Pt has also been found, because of weak interactions between the metal and the carbon support.[52]

The first reduction peak can be attributed to the coreduction of Pt and Re, indicating that Re is in close interaction with Pt. This promotion of the Re reduction can be caused by hydrogen spillover from the reduced Pt, which has been reported in the literature.[50,53−55]

The catalysts with the higher amount of Pt show both the lowest and the highest reduction peaks, indicating weak interactions between the metals. On the other hand, higher reduction temperatures for PRC11 and PRC13 could be due to strong Re−Pt interactions.[40] The intensity of the peaks increases as the Re content increases.

As observed from XRD and XPS results, reduction temperatures used for PRC catalysts result in complete reduction of Pt, while Re remains as an oxide. In the case of PRC31 with low Re loading, a certain amount of Re was reduced.

XPS analysis was performed for reduced PRC series catalysts to investigate the electronic state of platinum and rhenium on the surface.

Results (Figure 8, Table 4) showed mixed oxidation states for metals in all catalysts. A Pt $4f_{7/2}$ binding energy (BE) of 71.8 eV was assigned to Pt^0. These results are consistent with the BE values of 71.6 and 74.9 eV reported for a Pt 4f doublet

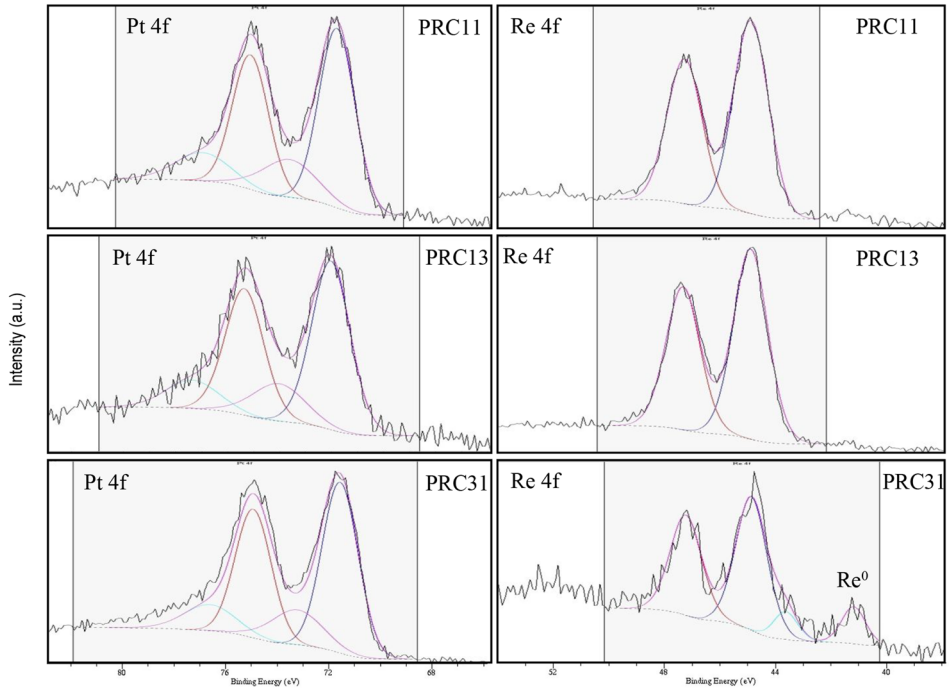

Figure 8. Pt 4f and Re 4f XPS spectra for PRC11, PCR13, and PRC31.

https://doi.org/10.1021/acs.energyfuels.1c02656
Energy Fuels 2021, 35, 17755−17768

Table 4. XPS Results for PRC Series Catalysts

	PRC13			PRC11			PRC31			
line	BE (eV)	fwhm (eV)	AC (at. %)	BE (eV)	fwhm (eV)	AC (at. %)	BE (eV)	fwhm (eV)	AC (at. %)	
C 1s	284.23	0.85	96.62	284.22	0.9	96.96	285.24	0.85	97.51[a]	C−C, sp_2
O 1s	530.2	1.45	1.39	530.3	1.45	1.38	530.7	1.9	0.96	Re═O
	531.4	1.5	0.39	531.6	1.5	0.56				Re−OH
	532.7	2.55	1.12	533.1	1.9	0.53	533.0	2.2	0.95	C−OH
							536.3	2.9	0.18	$\pi-\pi^*$ excitation
Pt 4f 7/2	72.0	1.7	0.14	71.8	1.55	0.22	71.7	1.55	0.33	Pt (0)
Re 4f 7/2							41.2	1	0.01	Re metal
	44.9	1.4	0.35	44.9	1.4	0.32	44.9	1.3	0.05	ReO_2
Re/Pt	2.5	1.45	0.46							

[a]Total carbon atomic concentration, including C−OH, vibrational structure, and $\pi-\pi^*$ excitation.

Scheme 1. General Reaction Scheme of Hydrodeoxygenation of Isoeugenol Using Pt and Pt−Re as Catalysts Supported on Carbon

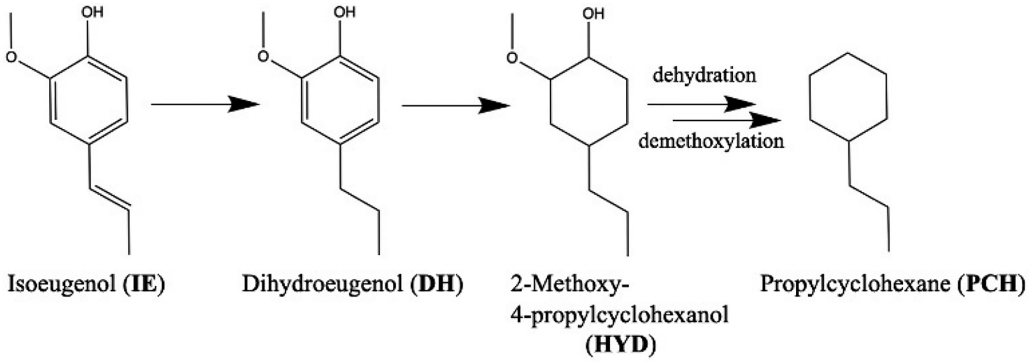

Table 5. Catalytic Activity of Pt and Pt−Re Catalysts Supported on Carbon in the Hydrodeoxygenation of Isoeugenol, Performed in a Batch Reactor

entry	catalyst	temperature, T (°C)	IE conversion after 4 h (%)[a]	liquid-phase mass balance (%)	PCH Y (%)	initial rate (mol/L h g_{Pt})
1	Pt/C1	200	100 (36)	82	<1	2.9
2	Pt/C1	300	100 (100)	32	31	4.7
3	Pt/C2	250	100 (71)	92	12	4.1
4	Pt/Norit	250	100 (23)	99	<1	
5	Pt/Sibunit	250	100 (<1)	99	<1	
6	PRC11	250	100 (98)	67	84	7.4
7	PRC31	250	100 (100)	62	66	15.4
8	PRC13	250	100 (100)	62	81	6.3

[a]Conversion of dihydroeugenol (DH) is shown in parentheses (DH X).

in metallic Pt.[56] The slight increase in BE after the addition of Re may indicate intermetallic interactions.

An Re 4f binding energy of 44.9 eV was assigned to Re^{4+}. This species was predominant for all catalysts. The catalyst with the lowest Re content, PRC 31, exhibited an additional signal at 41.2 eV, which was assigned for Re^0.[57] However, note that, since the measurements were done ex situ, the rhenium oxidation state can be influenced by exposure of highly oxophilic rhenium to ambient conditions.

The highest Re/Pt ratio was observed for PRC13 followed by PRC11 and thereafter PRC31.

Catalytic Activity. Monometallic Pt and bimetallic Pt−Re catalysts supported on carbon were tested in hydrodeoxygenation (HDO) of isoeugenol (IE). A general reaction scheme based on the reactants and products determined by GC and GC-MS is presented in Scheme 1.

Hydrogenation of the double bond located in the propene group of IE occurred almost immediately (after 1 min reaction time);[58] therefore, transformations of dihydroeugenol (DH) were followed.

Catalytic results and reaction conditions used for batch experiments with monometallic and bimetallic catalysts are summarized in Table 5. Two main products were found by GC and GC-MS: 2-methoxy-4-propylcyclohexanol, resulting from hydrogenation of the aromatic ring, and propylcyclohexane, the desired product of the aromatic ring hydrogenation and complete deoxygenation.

All catalysts were highly active for hydrogenation of the side-chain double bond of isoeugenol to form dihydroeugenol (DH), resulting in a complete isoeugenol conversion for all tested catalysts, however, propylcyclohexane yield (PCH Y) was low for monometallic Pt catalysts. On the other hand, bimetallic catalysts exhibited higher PCH Y values (80%−85%). Results will be discussed in more detail in the following sections.

https://doi.org/10.1021/acs.energyfuels.1c02656
Energy Fuels 2021, 35, 17755−17768

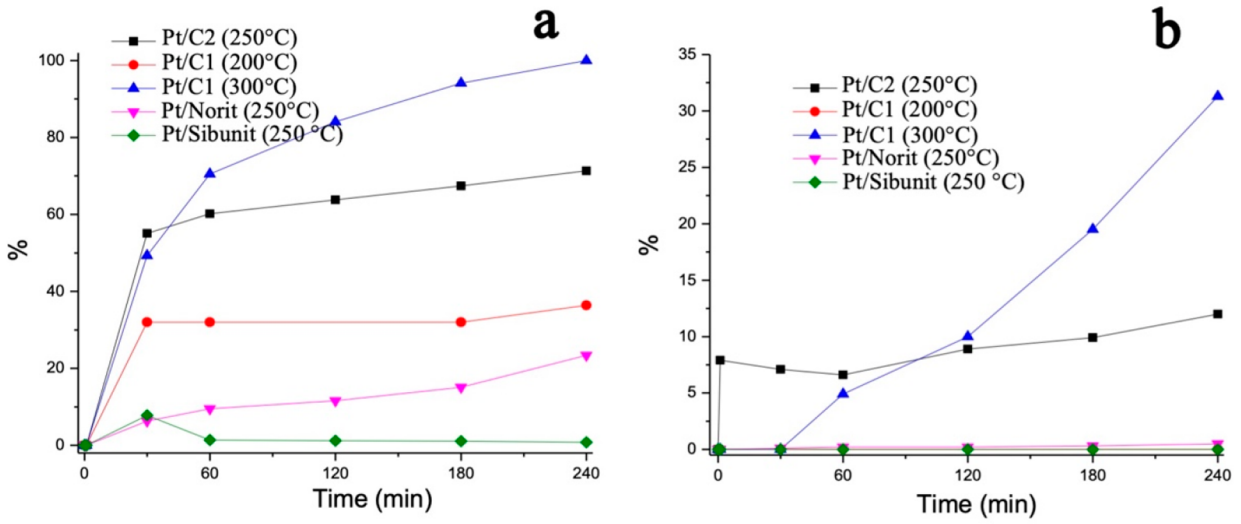

Figure 9. (a) Conversion of dihydroeugenol, as a function of time, and (b) yield of propylcyclohexane, as a function of time for monometallic Pt catalysts.

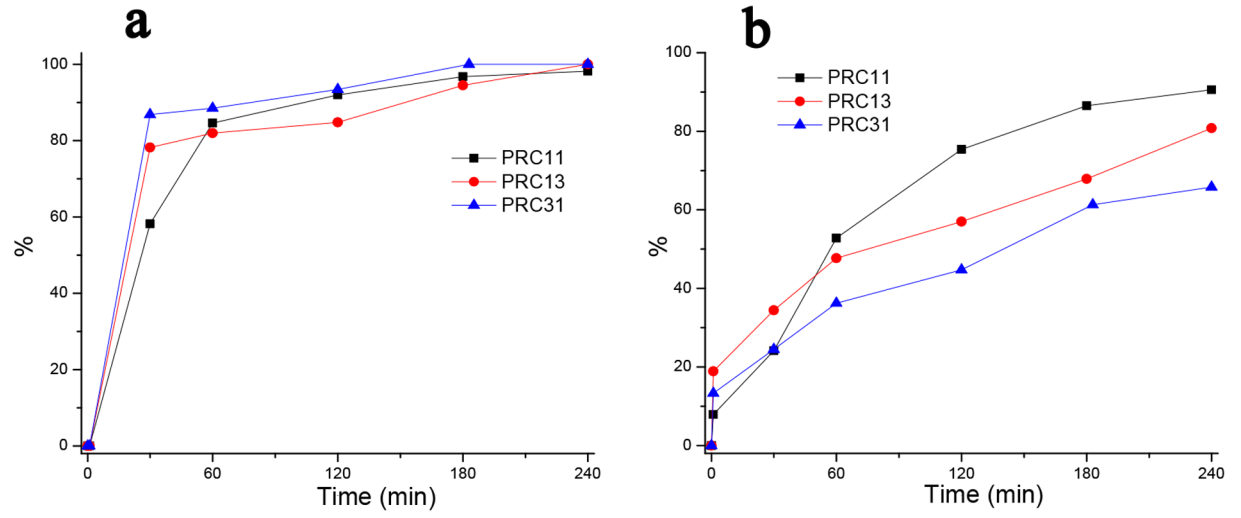

Figure 10. (a) Conversion of dihydroeugenol and (b) yield of propylcyclohexane, as a function of time for bimetallic Pt−Re catalysts.

All monometallic Pt catalysts displayed high hydrogenating activity of IE, being, however, poorly active in deoxygenation activity, as follows from Figure 9.

The lowest activity was obtained for the commercial catalyst Pt/C1 at 200 °C (Table 5, entry 1, at 4 h reaction time; DH X = 36%, PCH Y < 1%). The same catalyst was tested at 300 °C (Table 5, entry 2), resulting in the highest PCH Y (32%); however, the mass balance in the liquid phase at 4 h for reaction time was the lowest (32%), indicating that most products were distributed either in the gas phase, due to cracking, or as higher-molecular-weight polymers; neither of which was quantified.

The rest of the catalysts were tested at an intermediate temperature, 250 °C, to get better insight regarding their performance.

At 250 °C, the commercial catalyst Pt/C2 (Table 5, entry 3) exhibited a higher activity than Pt/Norit and Pt/Sibunit (Table 5, entries 4 and 5, respectively). This can be a result of catalyst acidity (Table 2), given that Pt/C2 has the highest acidity of all catalysts (pH of slurry 4.9). Both Pt/Norit and Pt/Sibunit displayed low deoxygenation activity, resulting in PCH Y < 1%.

As a comparison, monometallic Pt/C with pH 5.6 was not efficient in the HDO of guaiacol, giving mainly oxygenated products at 300 °C under 30 bar H_2.[59]

Bimetallic catalysts Pt−Re supported on Sibunit showed almost complete DH X (>98%) and a high PCH Y (>66%) (entries 6−8, Figure 10). Comparison of these results with monometallic Pt/Sibunit indicates that addition of Re had a noticeable effect on HDO activity, even if the slurry pH was not too acidic (Table 2).

Varying Pt:Re ratio also showed an effect on activity. While all PRC catalysts displayed almost complete conversion at 4 h of the reaction time, the lowest PCH Y (66%) was observed for PRC31.

Catalysts with a higher amount of Re, PRC11 and PRC13, had similar activity (PCH Y > 84%), with PRC11 displaying the highest PCH Y (84%) at 4 h. These results can be explained by the presence of ReOx (XPS results; see Figure 8) providing oxygen vacancies required for the deoxygenation to occur.[60]

The two best catalysts for HDO were PRC13 and PRC11; these results are consistent with a higher atomic concentration

https://doi.org/10.1021/acs.energyfuels.1c02656
Energy Fuels 2021, 35, 17755−17768

(AC) of Re on the surface of the catalysts and a predominant ReOx state, since it is necessary for oxygen activation. Moreover, their similar performance indicates that the amount of Pt has a lower effect on activity than the impact of Re, which is especially necessary for an inert support such as carbon.

For comparison, in a previous work[13] bimetallic PtRe/Al_2O_3 catalysts tested for HDO of isoeugenol under the same reaction conditions showed a lower PCH Y (54%) at 240 min. These results suggest that the choice of support plays a very important role. The use of Sibunit was not only beneficial for the metal dispersion and the particle size (6.5 nm for PtRe/Al_2O_3), but also had a positive effect on the activity of PtRe catalysts.

To explore the stability of the catalyst, repeatability and reusability tests were performed with PRC11 in a batch reactor at 250 °C and 30 bar of H_2. The obtained results are presented in Table 6 and Figure 11.

Table 6. Repeatability and Reusability Results for PRC11 in a Batch Reactor

catalyst	temperature, T (°C)	IE X after 4 h (%)[a]	liquid-phase mass balance (%)	PCH Y (%)
PRC11	250	100 (98)	70	91
PRC11 repeat	250	100 (100)	68	89
PRC11 reuse	250	100 (100)	67	84

[a]conversion of DH in parentheses (DH X).

From these tests, it can be seen that PRC11 displays consistent results when the reaction is repeated under the same conditions. Reusability tests were performed with the spent PRC11, which was washed with acetone and dried in air. The results show similar performance as with the fresh catalyst, indicating low catalyst deactivation.

A comparison of the results obtained in this work and those reported in the previous research is presented in Table 7. It can be observed that PCH yields and the mass balance in the liquid phase are higher for PRC11 and PRC13 catalysts under the same reaction conditions (250 °C, 30 bar H_2, and 4 h of reaction time).

Table 7. Comparison of Isoeugenol HDO under 250 °C, 30 bar H_2 and 4 h of Reaction Time with the Literature

catalyst	IE conversion after 4 h (%)[a]	liquid-phase mass balance (%)	PCH Y (%)	ref
PRC11	100 (98)	67	84	–
PRC31	100 (100)	62	66	–
PRC13	100 (100)	62	81	–
3, 1 wt % IrRe/Al_2O_3	100 (24)	53	69	13
10 wt % Ni/ZrO_2	100 (95)	15	16	31
3 wt % Ir/ZrO_2	100 (0)	37	33	31
10 wt % Ni/SBA-15	100 (100)	51	53	61

[a]conversion of DH in parentheses (DH X).

Granulated PRC11 was tested in a trickle-bed reactor to investigate scalability, stability, and the product distribution under a continuous flow (0.5 mL/min) of isoeugenol in dodecane at 30 bar H_2 and at 200, 170, 150, and 75 °C. The results are presented in Figure 12.

As it can be seen from Figure 12, IE X remained at 100% for all temperatures tested. DH X remained at 100% at temperatures of 200−150 °C; however, at 75 °C, it decreased to ca. 70%. The highest PCH Y was obtained at 200 °C (ca. 90%), concomitant with lowest mass balance in the liquid phase (ca. 75%).

PCH Y decreased as the temperature increased, from ca. 10% at 150 °C to ca. 50% at 170 °C. At 75 °C, PCH Y was <1%, indicating absence of deoxygenation at this temperature. This result is in accordance with the thermodynamics of IE HDO.[62]

The opposite results were recorded for HYD. At 200 °C, very low amounts of 2-methoxy-4-propylcyclohexanol were obtained (HYD Y ≈ 5%), whereas at 75 °C, it was the main product (ca. 60%). These results indicate that hydrogenation of the aromatic ring occurs efficiently at low temperatures, which is consistent with thermodynamics.[63] Consistent with the literature results, the activation energy (E_a) for hydrogenation of the aromatic ring is lower than the E_a value for deoxygenation.[47]

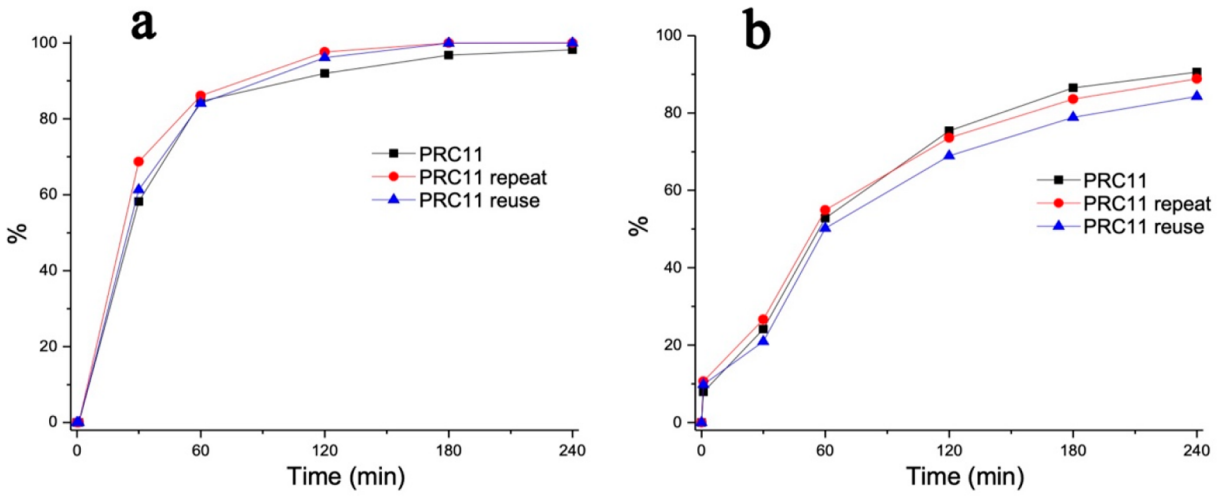

Figure 11. (a) Conversion of dihydroeugenol and (b) the yield of propylcyclohexane, as a function of time for PRC11 catalyst, repeatability, and reusability of the spent catalyst.

https://doi.org/10.1021/acs.energyfuels.1c02656
Energy Fuels 2021, 35, 17755−17768

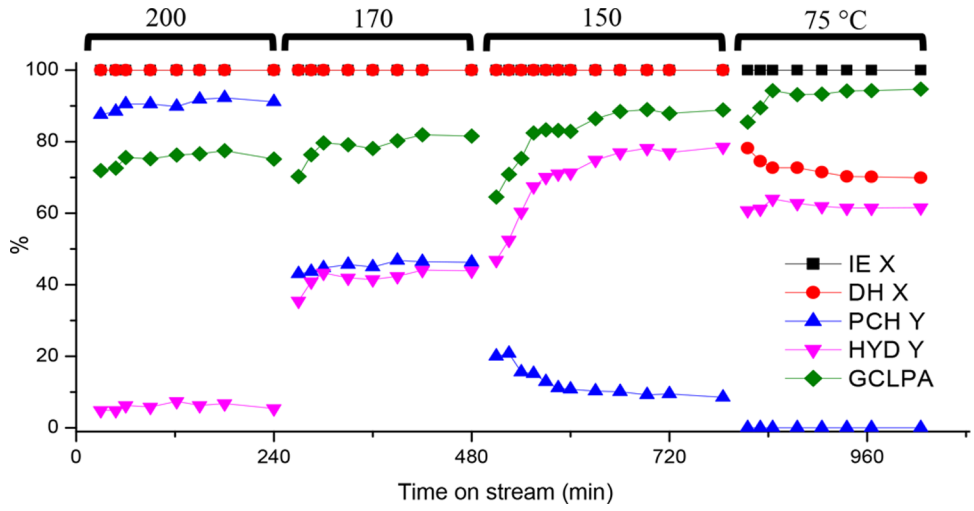

Figure 12. Continuous reactor results for HDO of isoeugenol performed at different temperatures, 30 bar H_2, and the liquid flow rate of 0.5 mL/min. Isoeugenol conversion (IE X), dihydroeugenol conversion (DH X), propylcyclohexane yield (PCH Y), 2-methoxy-4-propylcyclohexanol yield (HYD Y) and the liquid-phase mass balance (GCLPA).

Deactivation was not observed even after 17 h of time on stream, as conversion and yield remained constant.

A comparison between the batch and continuous results for PRC11 show that high conversion was achieved for both isoeugenol and dihydroeugenol, the mass balance in the liquid phase remained >60% and propylcyclohexane yield remained between 85% and 90%.

Apparent activation energy was calculated for isoeugenol HDO using the results at 60 min for experiments at different temperatures performed in the continuous reactor. From the Arrhenius plot presented in Figure 13, the apparent activation

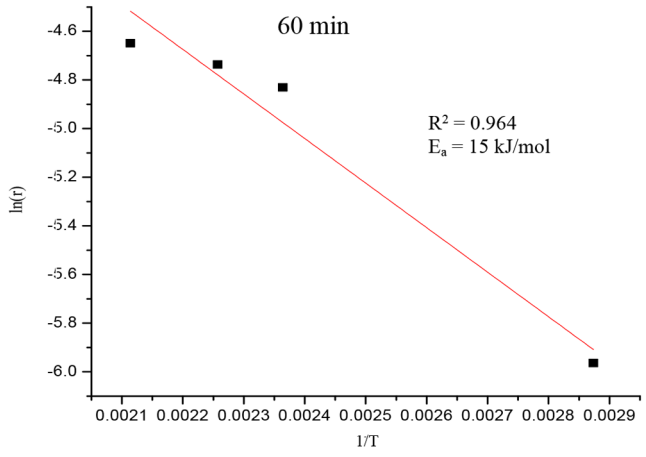

Figure 13. Arrhenius plot for the hydrodeoxygenation (HDO) of isoeugenol on granulated PtRe(1:1)/Sibunit. The slope gives the apparent activation energy of the reaction: E_a = 15 kJ/mol.

energy for HDO of IE using granulated PRC11 was determined to be 15 kJ/mol. This, along with visible changes in the slope upon temperature elevation, indicates that the presence of mass-transfer limitations in a continuous reactor with the catalyst particles exhibits a larger size than the counterparts applied in the batch reactor.

CONCLUSIONS

Hydrodeoxygenation (HDO) of isoeugenol was investigated at 200−300 °C under 30 bar of hydrogen pressure for the first time using monometallic commercial and synthesized catalysts, as well as bimetallic Pt−Re catalysts supported on mesoporous carbon.

For monometallic catalysts, commercial 5% Pt on active carbon catalyst showed the highest propylcyclohexane yield (31%) but the lowest mass balance in the liquid phase (32%) at 300 °C. At 250 °C, a similar catalyst exhibited higher propylcyclohexane yield and dihydroeugenol conversion, compared to less-acidic Pt/Norit and Pt/Sibunit.

Compared to monometallic Pt catalysts, bimetallic ones displayed higher activity for deoxygenation, giving complete conversion of isoeugenol and dihydroeugenol and resulting in high PCH Y at 250 °C and 30 bar H_2. PRC11 catalyst was the most active (isoeugenol conversion = 100%, dihydroeugenol conversion = 98%, propylcyclohexane yield = 84%) under the tested reaction conditions.

The best bimetallic catalysts were PRC11 and PRC13, which according to XPS contained ReOx species.

Granulated PRC11 was tested in a continuous trickle-bed reactor at 75−200 °C, 30 bar H_2, and 0.5 mL/min of liquid flow. This is the first study where the HDO of isoeugenol has been reported in the open literature in a continuous reactor. At low temperatures, the main product obtained was 2-methoxy-4-propylcyclohexanol, which indicated that deoxygenation was not occurring, however, complete conversion (100%) and a high yield of propylcyclohexane (ca. 90%) was obtained at 200 °C.

AUTHOR INFORMATION

Corresponding Author

Dmitry Yu. Murzin − *Johan Gadolin Process Chemistry Centre, Åbo Akademi University, Turku/Åbo FI-20500, Finland;* orcid.org/0000-0003-0788-2643; Email: dmurzin@abo.fi

https://doi.org/10.1021/acs.energyfuels.1c02656
Energy Fuels 2021, 35, 17755−17768

Authors

Mark E. Martínez-Klimov − *Johan Gadolin Process Chemistry Centre, Åbo Akademi University, Turku/Åbo FI-20500, Finland*

Päivi Mäki-Arvela − *Johan Gadolin Process Chemistry Centre, Åbo Akademi University, Turku/Åbo FI-20500, Finland;* orcid.org/0000-0002-7055-9358

Zuzana Vajglova − *Johan Gadolin Process Chemistry Centre, Åbo Akademi University, Turku/Åbo FI-20500, Finland*

Moldir Alda-Onggar − *Johan Gadolin Process Chemistry Centre, Åbo Akademi University, Turku/Åbo FI-20500, Finland*

Ilari Angervo − *Wihuri Physical Laboratory, Department of Physics and Astronomy, University of Turku, FI-20014 Turku, Finland*

Narendra Kumar − *Johan Gadolin Process Chemistry Centre, Åbo Akademi University, Turku/Åbo FI-20500, Finland*

Kari Eränen − *Johan Gadolin Process Chemistry Centre, Åbo Akademi University, Turku/Åbo FI-20500, Finland*

Markus Peurla − *Institute of Biomedicine, University of Turku, FI-20520 Turku, Finland*

Mehmet Harbi Calimli − *Johan Gadolin Process Chemistry Centre, Åbo Akademi University, Turku/Åbo FI-20500, Finland; Department of Medical Services and Techniques, Tuzluca Vocational School, University of Igdır, Igdır 76000, Turkey*

Joseph Muller − *Johan Gadolin Process Chemistry Centre, Åbo Akademi University, Turku/Åbo FI-20500, Finland*

Andrey Shchukarev − *Department of Chemistry, Umeå University, 901 87 Umeå, Sweden*

Irina L. Simakova − *Boreskov Institute of Catalysis, Novosibirsk 630090, Russia;* orcid.org/0000-0002-5138-4847

Complete contact information is available at: https://pubs.acs.org/10.1021/acs.energyfuels.1c02656

Notes

The authors declare no competing financial interest.

■ ACKNOWLEDGMENTS

Electron microscopy samples were processed and analyzed in the Electron Microscopy Laboratory, Institute of Biomedicine, University of Turku, which receives financial support from Biocenter Finland. I.S. is grateful for the support from the Ministry of Science and Higher Education of the Russian Federation, under the governmental order for Boreskov Institute of Catalysis (Project No. AAAAA21-121011390055-8). M.E.M.K. acknowledges the financial support received from the Magnus Ehrnrooth Foundation.

■ REFERENCES

(1) Ritchie, H., Roser, M. *Energy*; 2020. Published online at OurWorldInData.org. Available via the Internet at: https://ourworldindata.org/energy (accessed June 2, 2019).

(2) Markard, J. The Next Phase of the Energy Transition and its Implications for Research and Policy. *Nat. Energy.* **2018**, *3* (8), 628−633.

(3) Kammermann, J.; Bolvashenkov, I.; Tran, K.; Herzog, H. -G.; Frenkel, I. Feasibility Study for a Full-Electric Aircraft Considering Weight, Volume, and Reliability Requirements. In *2020 International Conference on Electrotechnical Complexes and Systems (ICOECS)*, 2020; pp 1−6, DOI: 10.1109/ICOECS50468.2020.9278461.

(4) Zhou, C.-H.; Xia, X.; Lin, C.-X.; Tong, D.-S.; Beltramini, J. Catalytic Conversion of Lignocellulosic Biomass to Fine Chemicals and Fuels. *Chem. Soc. Rev.* **2011**, *40* (11), 5588−5617.

(5) Meng, J.; Moore, A.; Tilotta, D.; Kelley, S.; Park, S. Toward Understanding of Bio-Oil Aging: Accelerated Aging of Bio-oil Fractions. *ACS Sustainable Chem. Eng.* **2014**, *2* (8), 2011−2018.

(6) Xiu, S.; Shahbazi, A. Bio-oil Production and Upgrading Research: A Review. *Renewable Sustainable Energy Rev.* **2012**, *16* (7), 4406−4414.

(7) Hu, X.; Gholizadeh, M. Progress of the Applications of Bio-Oil. *Renewable Sustainable Energy Rev.* **2020**, *134*, 110124.

(8) Mortensen, P. M.; Grunwaldt, J.-D.; Jensen, P. A.; Knudsen, K. G.; Jensen, A. D. A Review of Catalytic Upgrading of Bio-oil to Engine Fuels. *Appl. Catal., A* **2011**, *407* (1−2), 1−19.

(9) Mäki-Arvela, P.; Murzin, D. Y. Hydrodeoxygenation of Lignin-Derived Phenols: from Fundamental Studies Towards Industrial Applications. *Catalysts* **2017**, *7* (9), 265.

(10) He, Z.; Wang, X. Hydrodeoxygenation of Model Compounds and Catalytic Systems for Pyrolysis Bio-oils Upgrading. *Catal. Sustainable Energy* **2012**, *1*, 28−52.

(11) Laskar, D. D.; Tucker, M. P.; Chen, X.; Helms, G. L.; Yang, B. Noble-metal Catalyzed Cydrodeoxygenation of Biomass-Derived Lignin to Aromatic Hydrocarbons. *Green Chem.* **2014**, *16* (2), 897.

(12) Jin, W.; Pastor-Perez, L.; Shen, D.; Sepulveda-Escribano, A.; Gu, S.; Ramirez Reina, T. Catalytic Upgrading of Biomass Model Compounds: Novel Approaches and Lessons Learnt from Traditional Hydrodeoxygenation - a Review. *ChemCatChem* **2019**, *11* (3), 924−960.

(13) Luo, W.; Cao, W.; Bruijnincx, P. C. A.; Lin, L.; Wang, A.; Zhang, T. Zeolite-Supported Metal Catalysts for Selective Hydrodeoxygenation of Biomass-Derived Platform Molecules. *Green Chem.* **2019**, *21* (14), 3744−3768.

(14) Alda-Onggar, M.; Mäki-Arvela, P.; Eränen, K.; Aho, A.; Hemming, J.; Paturi, P.; Peurla, M.; Lindblad, M.; Simakova, I. L.; Murzin, D. Y. Hydrodeoxygenation of Isoeugenol Over Alumina Supported Ir-, Pt- and Re Catalysts. *ACS Sustainable Chem. Eng.* **2018**, *6* (12), 16205−16218.

(15) Teles, C. A.; Rabelo-Neto, R. C.; de Lima, J. R.; Mattos, L. V.; Resasco, D. E.; Noronha, F. B. The Effect of Metal Type on Hydrodeoxygenation of Phenol Over Silica Supported Catalysts. *Catal. Lett.* **2016**, *146* (10), 1848−1857.

(16) Horáček, J.; Kubička, D. Bio-Oil Hydrotreating Over Conventional CoMo and NiMo Catalysts: The role of Reaction Conditions and Additives. *Fuel* **2017**, *198*, 49−57.

(17) Jung, K. B.; Lee, J.; Ha, J.-M.; Lee, H.; Suh, D. J.; Jun, C.-H.; Jae, J. Effective Hydrodeoxygenation of Lignin-Derived Phenols Using Bimetallic RuRe catalysts: Effect of Carbon Supports. *Catal. Today* **2018**, *303*, 191−199.

(18) Liu, S.; Simonetti, T.; Zheng, W.; Saha, B. Selective Hydrodeoxygenation of Vegetable Oils and Waste Cooking Oils to Green Diesel Using a Silica-Supported Ir-ReO x Bimetallic Catalyst. *ChemSusChem* **2018**, *11* (9), 1446−1454.

(19) Liu, S.; Dutta, S.; Zheng, W.; Gould, N. S.; Cheng, Z.; Xu, B.; Saha, B.; Vlachos, D. G. Catalytic Hydrodeoxygenation of High Carbon Furylmethanes to Renewable Jet-fuel Ranged Alkanes over a Rhenium-Modified Iridium Catalyst. *ChemSusChem* **2017**, *10* (16), 3225−3234.

(20) Ota, N.; Tamura, M.; Nakagawa, Y.; Okumura, K.; Tomishige, K. Hydrodeoxygenation of Vicinal OH Groups over Heterogeneous Rhenium Catalyst Promoted by Palladium and Ceria Support. *Angew. Chem.* **2015**, *127* (6), 1917−1920.

(21) Zhang, J.; Zhao, C.; Li, C.; Li, S.; Tsang, C.-W.; Liang, C. The Role of Oxophilic Mo Species in Pt/MgO Catalyst as Extremely Active Sites for Enhanced Hydrodeoxygenation of Dibenzofuran. *Catal. Sci. Technol.* **2020**, *10*, 2948−2960.

(22) Goulas, K. A.; Mironenko, A. V.; Jenness, G. R.; Mazal, T.; Vlachos, D. G. Fundamentals of C−O Bond Activation on Metal Oxide Catalysts. *Nat. Catal.* **2019**, *2*, 269−276.

(23) Fang, H.; Zheng, J.; Luo, X.; Du, J.; Roldan, A.; Leoni, S.; Yuan, Y. Product Tunable Behavior of Carbon Nanotubes-Supported Ni−Fe catalysts for Guaiacol Hydrodeoxygenation. *Appl. Catal., A* **2017**, *529*, 20−31.
(24) Tran, N. T. T.; Uemura, Y.; Ramli, A. Hydrodeoxygenation of Guaiacol over Al-MCM-41 Supported Metal Catalysts: A Comparative Study of Co and Ni. *Procedia Eng.* **2016**, *148*, 1252−1258.
(25) Vargas-Villagrán, H.; Flores-Villeda, M. A.; Puente-Lee, I.; Solís-Casados, D. A.; Gómez-Cortés, A.; Díaz-Guerrero, G.; Klimova, T. E. Supported Nickel Catalysts for Anisole Hydrodeoxygenation: Increase in the Selectivity to Cyclohexane. *Catal. Today* **2020**, *349*, 26−41.
(26) Jung, K. B.; Lee, J.; Ha, J.-M.; Lee, H.; Suh, D. J.; Jun, C.-H.; Jae, J. Effective Hydrodeoxygenation of Lignin-Derived Phenols Using Bimetallic RuRe Catalysts: Effect of Carbon Supports. *Catal. Today* **2018**, *303*, 191−199.
(27) Plaksin, G. V.; Baklanova, O. N.; Lavrenov, A. V.; Likholobov, V. A. Carbon Materials from the Sibunit Family and Methods for Controlling Their Properties. *Solid Fuel Chem.* **2014**, *48* (6), 349−355.
(28) Lokteva, E. S.; Lunin, V. L.; Golubina, E. V.; Simagina, V. I.; Egorova, M.; Stoyanova, I. V. C-C Bond Formation During Hydrodechlorination of CCl_4 on Pd-Containing Catalysts. *Stud. Surf. Sci. Catal.* **2000**, *130*, 1997−2002.
(29) Baklanova, O. N.; Likholobov, V. A.; Tsekhanovich, M. S.; Davydova, V. Y.; Chirkova, O. A.; Drozdov, V. A.; Surovikin, Y. V. Effect of the Particle Size of Globular Nanodisperse Carbon on the Texture and Strength of Molded Sibunit-Type Materials. *Catal. Ind.* **2009**, *1* (2), 153−156.
(30) Fenelonov, V. B.; Likholobov, V. A.; Derevyankin, A. Y.; Mel'gunov, M. S. Porous Carbon Materials Prepared from C1-C3 Hydrocarbons. *Catal. Today* **1998**, *42*, 341.
(31) Gaillard, F.; Hachimi, A. E.; Descorme, C.; Besson, M.; Joly, J.-P.; Polyanskaya, E. M.; Taran, O. P.; Parmon, V. N. Study of oxygen groups at a porous carbon surface by a new fast intermittent thermodesorption technique. *Carbon* **2011**, *49* (6), 2062−2073.
(32) Costandy, J. G.; Edgar, T. F.; Baldea, M. Switching from Batch to Continuous Reactors is a Trajectory Optimization Problem. *Ind. Eng. Chem. Res.* **2019**, *58* (30), 13718−13736.
(33) Roberts, E. J.; Habas, S. E.; Wang, L.; Ruddy, D. A.; White, E. A.; Baddour, F. G.; Griffin, M. B.; Schaidle, J. A.; Malmstadt, N.; Brutchey, R. L. High-Throughput Continuous Flow Synthesis of Nickel Nanoparticles for the Catalytic Hydrodeoxygenation of Guaiacol. *ACS Sustainable Chem. Eng.* **2017**, *5* (1), 632−639.
(34) Yan, P.; Li, M. M.-J.; Adesina, A. A.; Zhao, G.; Setiawan, A.; Kennedy, E. M.; Stockenhuber, M. The Role of Acid and Metal Sites in Hydrodeoxygenation of Guaiacol over Ni/Beta Catalysts. *Catal. Sci. Technol.* **2020**, *10*, 810−825.
(35) Duval, A.; Lawoko, M. A Review on Lignin-Based Polymeric, Micro- and Nano-structured Materials. *React. Funct. Polym.* **2014**, *85*, 78−96.
(36) Alda-Onggar, M.; Mäki-Arvela, P.; Aho, A.; Simakova, I. L.; Murzin, D. Y. Hydrodeoxygenation of Phenolic Model Compounds over Zirconia Supported Ir and Ni-Catalysts. *React. Kinet., Mech. Catal.* **2019**, *126*, 737−759.
(37) Coloma, F.; Sepúlveda-Escribano, A.; Rodríguez-Reinoso, F. Heat-Treated Carbon-Blacks as Supports for Platinum Catalysts. *J. Catal.* **1995**, *154* (2), 299−305.
(38) Sepúlveda-Escribano, A.; Coloma, F.; Rodríguez-Reinoso, F. Platinum Catalysts Supported on Carbon Blacks with Different Surface Chemical Properties. *Appl. Catal., A* **1998**, *173* (2), 247−257.
(39) Moreno-Castilla, C.; Carrasco-Marín, F.; Parejo-Pérez, C.; López Ramon, M. Dehydration of Methanol to Dimethyl Ether Catalyzed by Oxidized Activated Carbons with Varying Surface Acidic Character. *Carbon* **2001**, *39* (6), 869−875.
(40) Wang, S.; Lu, G. Q. Effects of Acidic Treatments on the Pore and Aurface Properties of Ni Catalyst Supported on Activated Carbon. *Carbon* **1998**, *36* (3), 283−292.
(41) Zazo, J. A.; Fraile, A. F.; Rey, A.; Bahamonde, A.; Casas, J. A.; Rodriguez, J. J. Optimizing Calcination Temperature of Fe/Activated Carbon Catalysts for CWPO. *Catal. Today* **2009**, *143* (3−4), 341−346.
(42) Markus, H.; Mäki-Arvela, P.; Kumar, N.; Kul'kova, N. V.; Eklund, P.; Sjöholm, R.; Holmbom, B.; Salmi, T.; Murzin, D. Y. Hydrogenolysis of Hydroxymatairesinol over Carbon-Supported Palladium Catalysts. *Catal. Lett.* **2005**, *103* (1−2), 125−131.
(43) Kovalenko, G. A.; Rudina, N. A.; Perminova, L. V.; Chuenko, T. V.; Skrypnik, O. V. Preparation and Characterization of Nanoporous Carbon Supports on a Nickel/Sibunit Catalyst. *Kinet. Catal.* **2009**, *50* (4), 597−605.
(44) Leofanti, G.; Padovan, M.; Tozzola, G.; Venturelli, B. Surface Area and Pore Texture of Catalysts. *Catal. Today* **1998**, *41* (1−3), 207−219.
(45) Lopez-Ruiz, J. A.; Davis, R. J. Decarbonylation of Heptanoic Acid over Carbon-Supported Platinum Nanoparticles. *Green Chem.* **2014**, *16* (2), 683−694.
(46) Qiu, T.; Yang, J.-G.; Bai, X.-J.; Wang, Y.-L. The Preparation of Synthetic Graphite Materials with Hierarchical Pores from Lignite by One-Step Impregnation and Their Characterization as Dye Absorbents. *RSC Adv.* **2019**, *9* (22), 12737−12746.
(47) Borisov, V. A.; Iost, K. N.; Temerev, V. L.; Surovikin, Y. V.; Smorokov, A. A.; Fedotova, P. A.; Shlyapin, D. A. High-Temperature Modification of Sibunit for its Application as a Support for Ruthenium Catalysts in Ammonia Synthesis. *AIP Conf. Proc.* **2018**, *2141*, 020017.
(48) Godina, L. I.; Kirilin, A. V.; Tokarev, A. V.; Simakova, I. L.; Murzin, D. Y. Sibunit-Supported Mono- and Bimetallic Catalysts Used in Aqueous-Phase Reforming of Xylitol. *Ind. Eng. Chem. Res.* **2018**, *57*, 2050−2067.
(49) Yentekakis, I. V.; Goula, G.; Panagiotopoulou, P.; Kampouri, S.; Taylor, M. J.; Kyriakou, G.; Lambert, R. M. Stabilization of Catalyst Particles Against Sintering on Oxide Supports with High Oxygen Ion Lability Exemplified by Ir- Catalyzed Decomposition of N_2O. *Appl. Catal., B* **2016**, *192*, 357−364.
(50) Chen, N.-Y.; Liu, M.-C.; Yang, S.-C.; Chang, J.-R. EXAFS Peaks and TPR Characterizing Bimetallic Interactions: Effects of Impregnation Methods on the Structure of Pt-Ru/C Catalysts. *J. Spectrosc.* **2014**, *2014*, 1−12.
(51) Di, X.; Li, C.; Lafaye, G.; Especel, C.; Epron, F.; Liang, C. Influence of Re−M Interactions in Re−M/C Bimetallic Catalysts Prepared by a Microwave-Assisted Thermolytic Method on Aqueous-Phase Hydrogenation of Succinic Acid. *Catal. Sci. Technol.* **2017**, *7* (22), 5212−5223.
(52) Simonetti, D.; Kunkes, E.; Dumesic, J. Gas-Phase Conversion of Glycerol to Synthesis Gas over Carbon-Supported Platinum and Platinum−Rhenium Catalysts. *J. Catal.* **2007**, *247* (2), 298−306.
(53) Conner, W. C.; Falconer, J. L. Spillover in Heterogeneous Catalysis. *Chem. Rev.* **1995**, *95* (3), 759−788.
(54) Prins, R. Hydrogen Spillover. Facts and Fiction. *Chem. Rev.* **2012**, *112* (5), 2714−2738.
(55) Nakagawa, Y.; Tazawa, S.; Wang, T.; Tamura, M.; Hiyoshi, N.; Okumura, K.; Tomishige, K. Mechanistic Study of Hydrogen-Driven Deoxydehydration over Ceria-Supported Rhenium Catalyst Promoted by Au Nanoparticles. *ACS Catal.* **2018**, *8* (1), 584−595.
(56) Fan, J.; Qi, K.; Zhang, L.; Zhang, H.; Yu, S.; Cui, X. Engineering Pt/Pd Interfacial Electronic Structures for Highly Efficient Hydrogen Evolution and Alcohol Oxidation. *ACS Appl. Mater. Interfaces* **2017**, *9* (21), 18008−18014.
(57) *Handbook of X-ray Photoelectron Spectroscopy*; Chastain, J., King, R. C., Jr., Eds.; Physical Electronics, Inc., 1995; 261 pp.
(58) Lindfors, C.; Mäki-Arvela, P.; Paturi, P.; Aho, A.; Eränen, K.; Hemming, J.; Peurla, M.; Kubicka, D.; Simakova, I. L.; Murzin, D. Y. Hydrodeoxygenation of Isoeugenol over Ni- and Co-Supported Catalysts. *ACS Sustainable Chem. Eng.* **2019**, *7* (17), 14545−14560.
(59) Sulman, A.; Mäki-Arvela, P.; Bomont, L.; Alda-Onggar, M.; Fedorov, V.; Russo, V.; Eränen, K.; Peurla, M.; Akhmetzyanova, U.; Skuhrovcová, L.; Tišler, Z.; Grénman, H.; Wärnå, J.; Murzin, D. Y.

https://doi.org/10.1021/acs.energyfuels.1c02656
Energy Fuels 2021, 35, 17755−17768

Kinetic and Thermodynamic Analysis of Guaiacol Hydrodeoxygenation. *Catal. Lett.* **2019**, *149* (9), 2453−2467.
(60) Alvarez, C.; Cruces, K.; Garcia, R.; Sepulveda, C.; Fierro, J. L. G.; Ghampson, I. T.; Escalona, N. Conversion of Guaiacol over Different Re Active Phases Supported on CeO_2-Al_2O_3. *Appl. Catal., A* **2017**, *547*, 256−264.
(61) Tieuli, S.; Mäki-Arvela, P.; Peurla, M.; Eränen, K.; Wärnå, J.; Cruciani, G.; Menegazzo, F.; Murzin, D. Y.; Signoretto, M. Hydrodeoxygenation of Isoeugenol over Ni-SBA-15: Kinetics and Modelling. *Appl. Catal., A* **2019**, *580*, 1−10.
(62) Bomont, L.; Alda-Onggar, M.; Fedorov, V.; Aho, A.; Peltonen, J.; Eränen, K.; Peurla, M.; Kumar, N.; Wärnå, J.; Russo, V.; et al. Production of Cycloalkanes in Hydrodeoxygenation of Isoeugenol over Pt- and Ir-Modified Bifunctional Catalysts. *Eur. J. Inorg. Chem.* **2018**, *2018*, 2841−2854.
(63) Temkin, M. I.; Murzin, D. Y.; Kul'kova, N. V. Kinetics and Mechanism of Liquid-Phase Hydrogenation. *Doklady Acad. Sci. USSR* **1988**, *303*, 659.

https://doi.org/10.1021/acs.energyfuels.1c02656
Energy Fuels 2021, 35, 17755−17768